DEPARTMENT OF COMMERCE
LUTHER H. HODGES, Secretary

WEATHER BUREAU
F. W. REICHELDERFER, Chief

MONTHLY WEATHER REVIEW

JAMES E. CASKEY, JR., Editor

Volume 89, Number 11 | Washington, D.C. | November 1961

ANALYSIS OF SATELLITE INFRARED RADIATION MEASUREMENTS ON A SYNOPTIC SCALE [1, 2]

MELVIN WEINSTEIN, LT. COL., USAF [3]
Air Weather Service
and
VERNER E. SUOMI
University of Wisconsin, Madison, Wis.

[Manuscript received May 22, 1961; revised September 12, 1961]

ABSTRACT

Long-wave radiation loss maps, based on Explorer VII measurements of terrestrial radiation at night, are analyzed and compared with composite nephanalyses and frontal analyses. Results indicate a definite relationship between the radiation centers and their corresponding surface low and high pressure centers, their locations, 24-hour intensifications and movements, and the conformity of these movements to the 500-mb. geostrophic flow. Some of the potential applications to analysis and forecasting are noted.

1. INTRODUCTION

The radiation-balance experiment aboard the International Geophysical Year satellite, 1959 Iota (Explorer VII) was developed by a University of Wisconsin team and is described in [8].

The primary purpose of the experiment is to measure the solar, reflected, and terrestrial radiation currents to obtain the radiant heat flow to and from the earth, and ultimately to obtain a clearer understanding of the driving force behind the circulation of the atmosphere. Observations of the long-wave radiation currents from the shadow zone portion of the earth measured by the omnidirectional bolometer were used to draw composite radiation loss maps. The relationship of these maps to other meteorological analyses and parameters and their application to analysis and forecasting are described in this paper.

[1] This research was supported by the National Aeronautics and Space Administration under contract no. NASw-65 and the National Academy of Sciences as part of the International Geophysical Year.

[2] A portion of the material contained in this paper is from a thesis by Melvin Weinstein submitted in partial fulfillment of the requirements for the degree of Master of Science at the University of Wisconsin.

[3] Present address Air Weather Service Member, Meteorological Satellite Laboratory, U.S. Weather Bureau, Washington 25, D.C.

2. LONG-WAVE RADIATION LOSS MAPS

RADIATION OBSERVATIONS

The satellite's orbit is inclined 50.3° to the earth's equator and varies in altitude from 1,100 km. at apogee to 550 km. at perigee. During the period studied, early December 1959, the satellite came out of the sun at 50° N., traveled southeastward and entered the sunlight zone in the Southern Hemisphere. The orbital period is 101 minutes and radiation observations are taken every 42 seconds, during which the satellite travels 2.5° of latitude (fig. 1). Limitations of this orbit are the restriction of observations to between 50° N. and S., the variation of local time along the orbit, and scarcity of observations at lower latitudes.

The spherical sensor integrates the radiation received from the entire field of view. The amount received from a unit area of the earth is weighted according to its position with respect to the satellite, being inversely proportional to the square of the distance from the point on earth to the satellite and directly proportional to the cosine of the angle between the local zenith and a line to the satellite as observed from that point [3]. For example, at satellite altitude of 700 km. the total radius

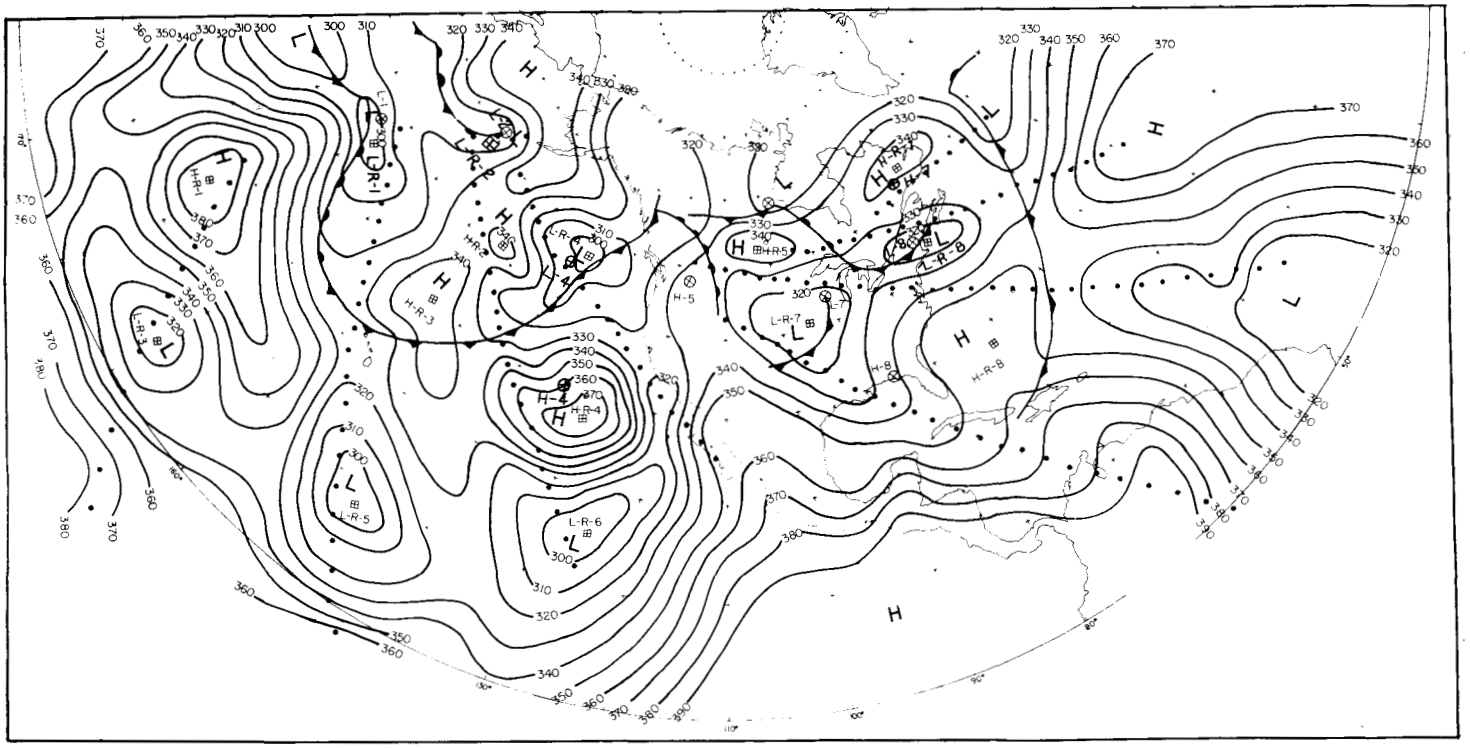

FIGURE 1.—Long-wave radiation loss map, December 1, 1959. Lines are isolangleys, connecting equal long-wave radiation loss values in Langleys per minute $\times 10^{-3}$. Surface pressure centers and fronts are composite to the satellite passage time. Surface pressure centers, marked by circles, are designated L for Low and H for High, plus an Arabic number (thus L–1). Radiation centers, marked by squares, are distinguished from surface centers by the inclusion of R (thus L–R–1 is radiation Low number 1 which is associated with surface Low L–1). Satellite observation points and orbit path are shown by dots.

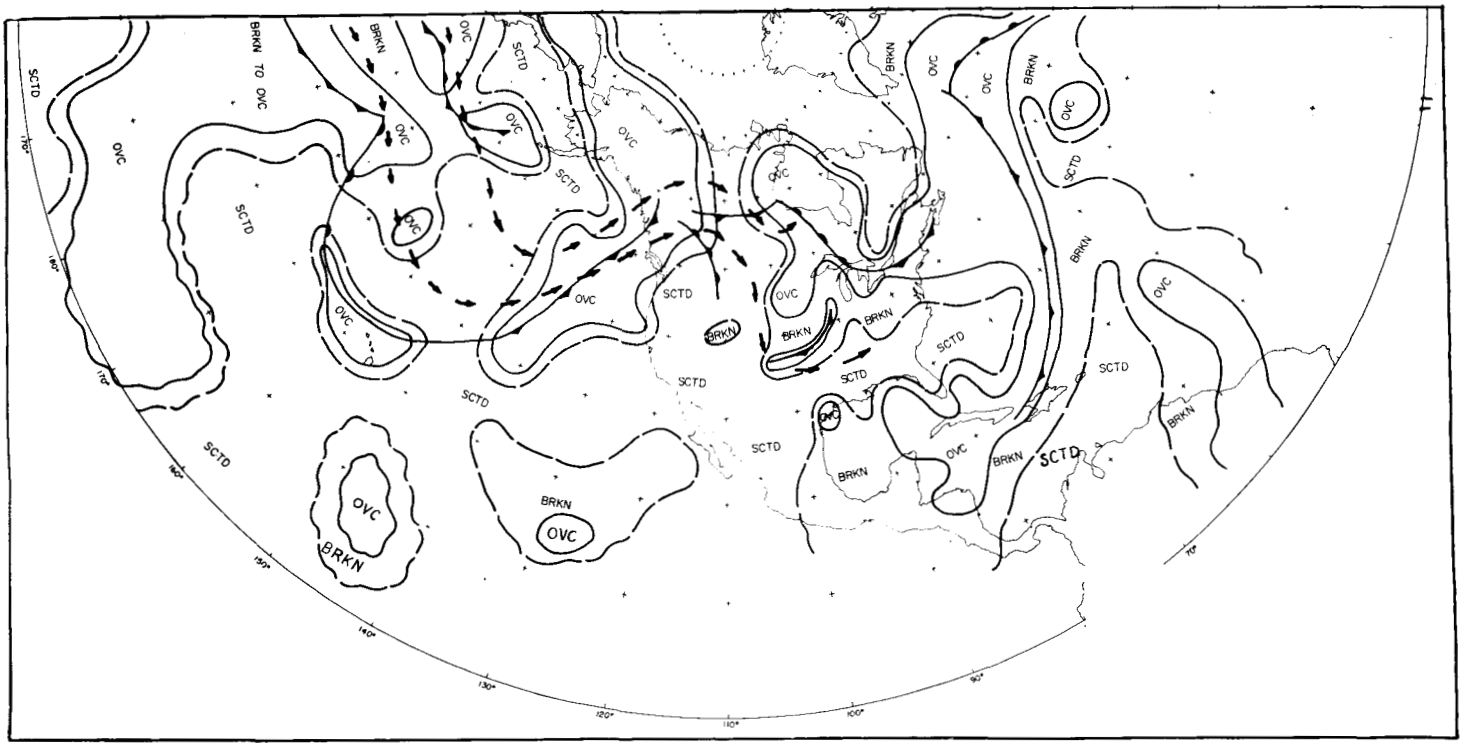

FIGURE 2.—Composite nephanalysis, December 1, 1959, based on 0000, 0600, and 1200 GMT surface maps. Overcast (OVC) areas are enclosed within solid lines. Broken lines separate the clear to scattered (SCTD) areas from the broken, 5/8 to 7/8 (BRKN). Wavy lines indicate the actual cloud area edge is unknown due to lack of data. Arrows show regions of maximum winds, from the 0000 GMT, 300-mb. chart.

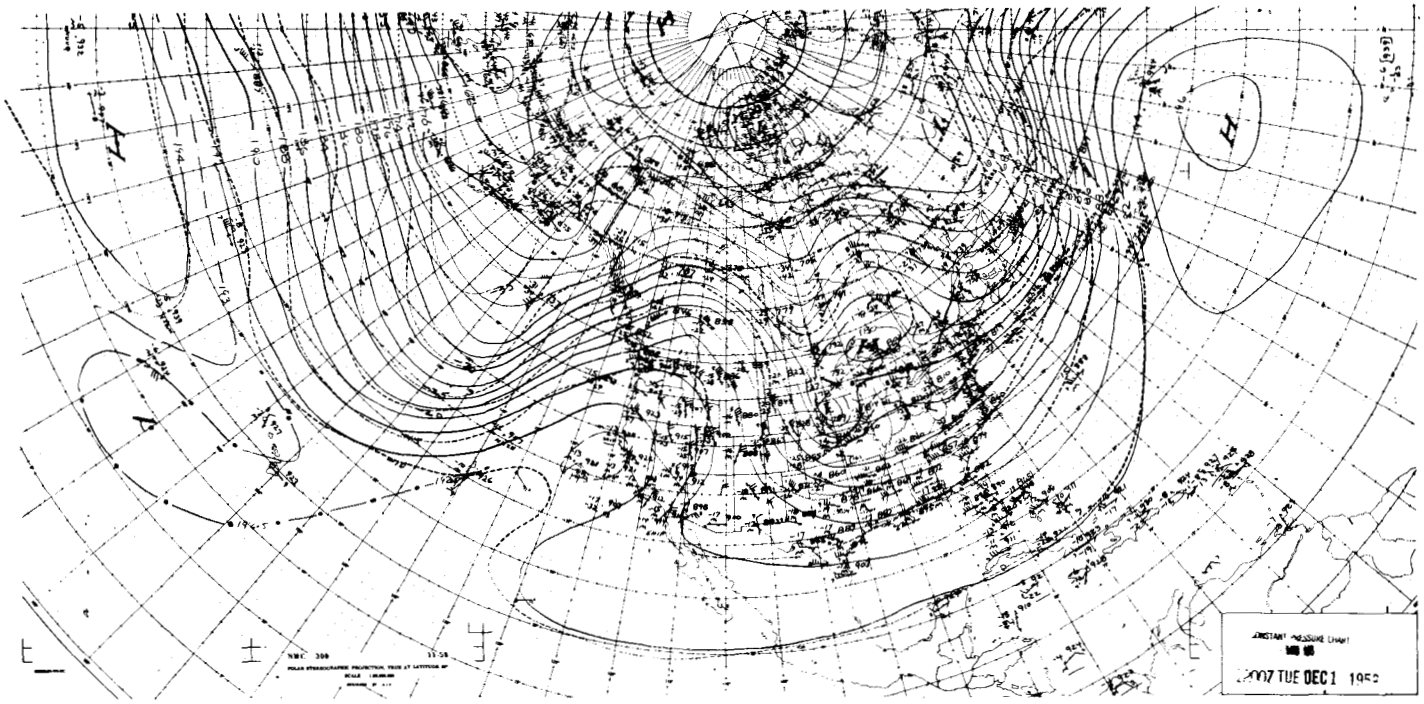

FIGURE 3.—500-mb. map, 1200 GMT, December 1, 1959.

of the circular area viewed on the earth is 25.8° of latitude (2,855 km.) measured from the subsatellite point. However, 50 percent of the radiation comes from a relatively small area whose radius is 6.6° of latitude and which comprises only 7.6 percent of the total area viewed. Nine-tenths of the radiation comes from only 33.2 percent of the area viewed [4]. As a result, the changes in radiation are heavily weighted toward the area just below the satellite.

The surface of the earth or of a cloud radiates essentially as a black body. A portion of this radiation is transmitted through the atmosphere and the remainder is absorbed by atmospheric gases, principally CO_2, H_2O, and O_3. The atmosphere itself reradiates energy. In fact, most of the energy leaving the top of the atmosphere comes from the atmosphere itself. Nocturnal radiation measurements were used in this study because radio reception from the satellite is much better at night when there is greater ionospheric transparency. This results in more data and better global coverage. In addition, calculations for the nighttime case are much simpler because the white hemisphere is measuring only long-wave radiation.

The bolometer is a thin hemispherical shell thermally isolated from a mirror large enough so that no part of the satellite itself is seen by the bolometer. Since the satellite is spinning rapidly on an axis parallel to the mirror surface, the hemispherical bolometer acts like a sphere in space. The heat transfer by conduction and long-wave radiation to the mirror is small but not negligible compared to radiative transfer from the earth and to space. The energy balance equation for a spinning mirror-backed hemisphere in space in the shadow zone of the earth reduces to

$$\alpha\beta\frac{R\uparrow}{2}=2\pi\epsilon\sigma T_w^4-H\frac{\partial T}{\partial t}-K(T_w-T_m) \tag{1}$$

$$R\uparrow=\frac{1}{\beta}\left[\frac{4\pi\epsilon\sigma T_w^4}{\alpha}-\frac{2H}{\alpha}\frac{\partial T}{\partial t}-\frac{2K}{\alpha}(T_w-T_m)\right] \tag{2}$$

where $R\uparrow$ is the total radiation received by the bolometer, β is the solid angle to the earth, α and ϵ are the infrared absorptivity and emissivity of the sensor, σ the Stefan-Boltzmann constant, H a term equivalent to the time constant of the sensor, and K the thermal conductivity between the temperatures of the sensor (T_w) and the mirror (T_m).

Actually H is a function of temperature because the heat transfer process, principally radiation, is temperature dependent. K is also temperature dependent because there is radiation exchange between the inside of the hemisphere and the mount. However, in order to simplify the hand calculations, both H and K are assumed to be constant. Even so, since $\alpha=\epsilon$ from Kirchoff's law, the value of the first term in the brackets, the greatest of the three, is determined by the absolute temperature T_w. A most pessimistic value of its error would be ± 1 °C.; a more likely value is about one-fourth of that. However, even an error of 1° C. would give rise to an error of only 2.5 percent in the final value of $R\uparrow$. The satellite altitude and therefore the solid angle β is known to good accuracy. An error of 100 percent in K will give an error of 10 percent in the final result. Finally, while at equilibrium the second term goes to zero, it might be significant

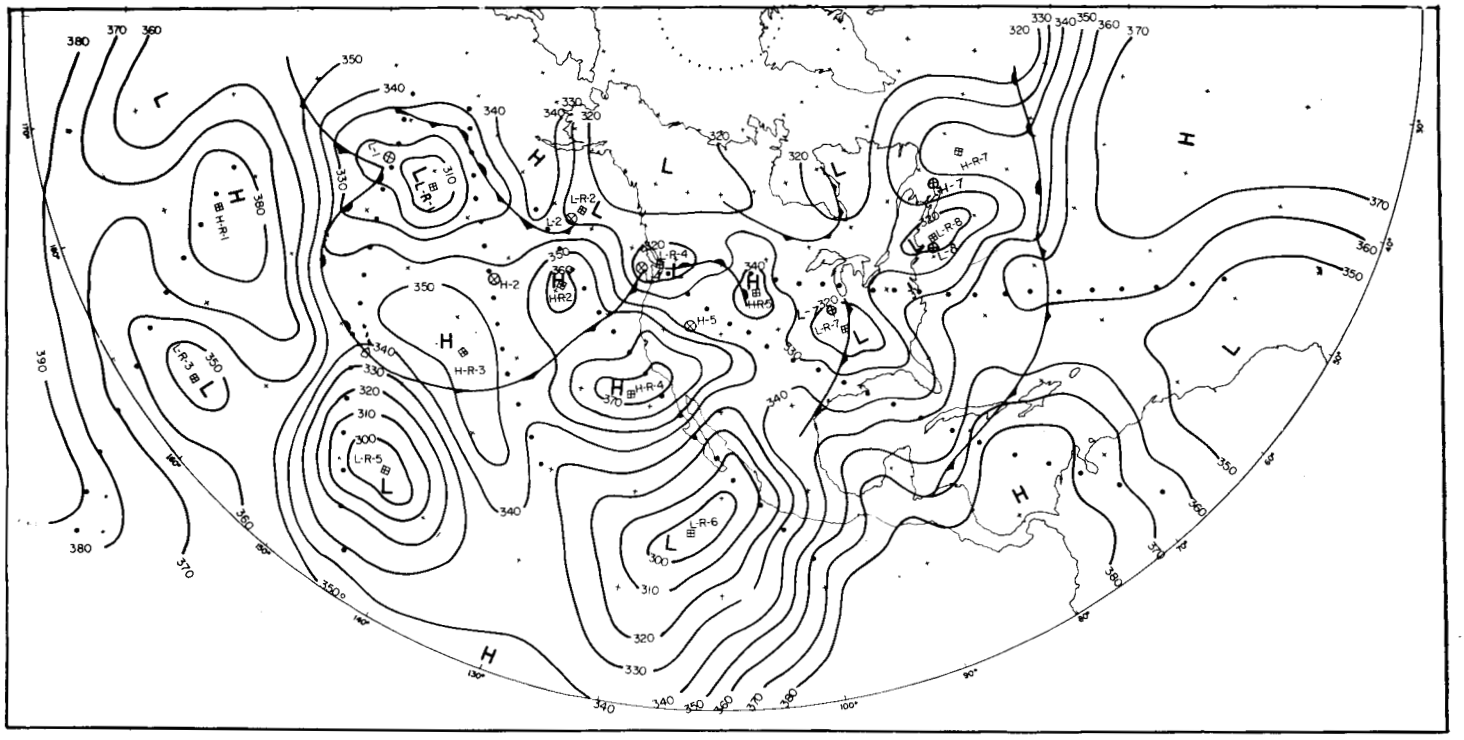

FIGURE 4.—Long-wave radiation loss map, December 2, 1959. (See fig. 1 for legend.)

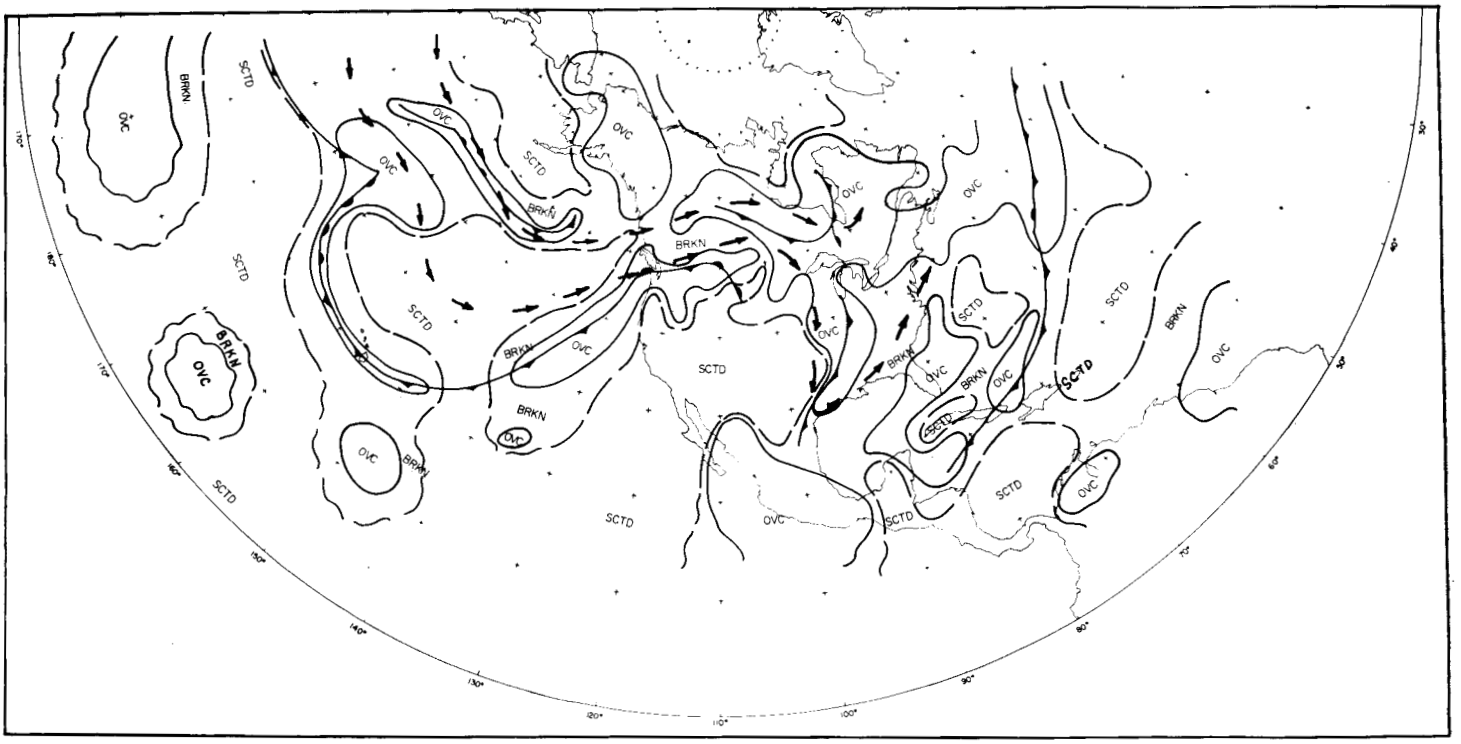

FIGURE 5.—Composite nephanalysis, December 2, 1959. (See fig. 2 for legend.)

just as the satellite comes out of the sun. One is tempted to say, therefore, that the radiation values at 50° N. are probably too high. Our feeling is that it is best to await the more complete calculations being done on a computer. However, it will be a surprise if they differ by more than 10 percent from what we are showing here. In any case these results are sufficient to show changes in the patterns of outgoing radiation.

Thus the radiation observation values used in the long-wave radiation maps are probably within 10 percent of the absolute values. However, the values for three maps which do not cover the complete hemisphere should

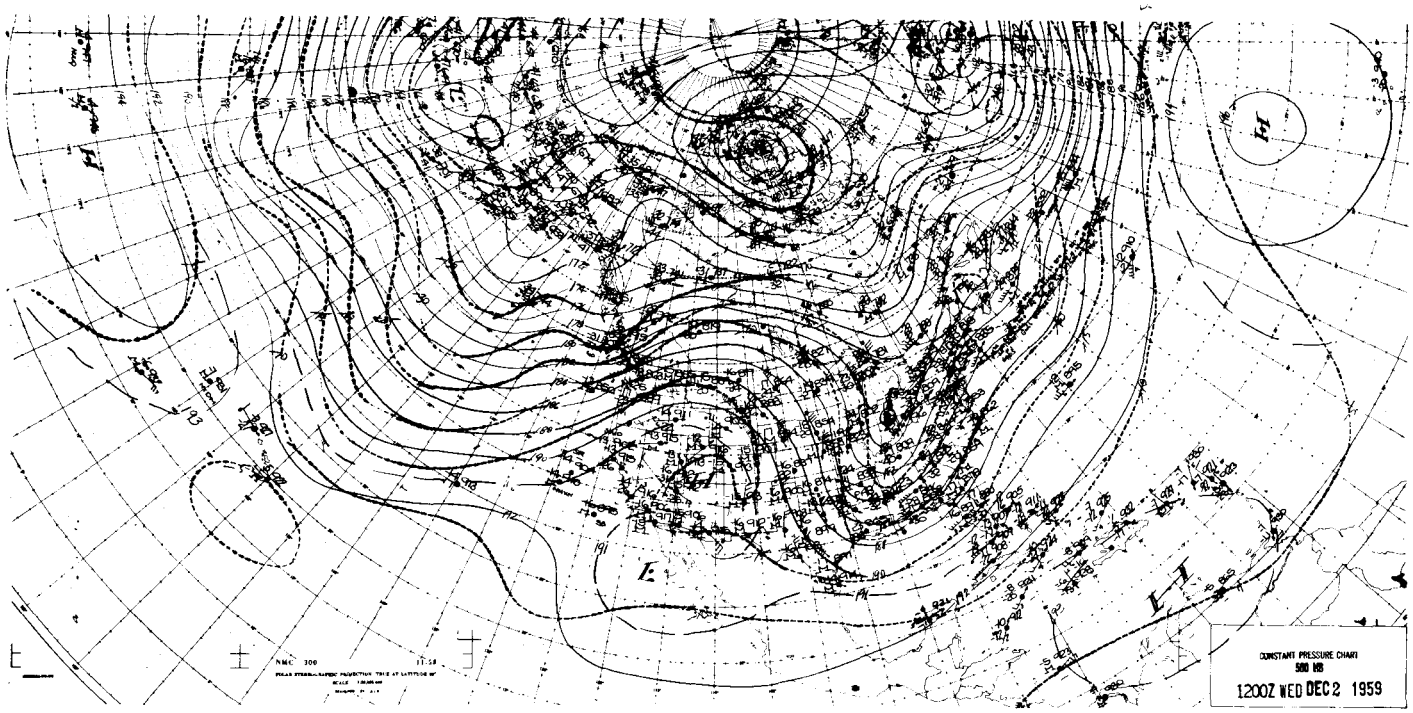

FIGURE 6.—500-mb. map, 1200 GMT, December 2, 1959.

not be used for comparison with average hemispheric values. From a synoptic point of view, the radiation observations are extremely useful because they are comparable to each other relatively so that the radiation patterns and their continuity have meaning.

ANALYSIS PROCEDURE

Because the spherical sensor integrates the radiation over a large segment of the earth, it is possible to draw a composite radiation map using data from successive satellite orbit paths, even though there is a time difference of 1 hour and 40 minutes between orbit paths. Lines of equal long-wave radiation loss, in Langleys per minute $\times 10^{-3}$ (isolangleys) are drawn on the radiation map, using the same principles as those for drawing isobars on a surface map or contours on an upper air map.

Since the radiation maps are not synoptic, composite surface frontal and nephanalysis maps, which coincide as closely as possible with the times of the radiation observations, are constructed based on National Weather Analysis Center analyses. The composite nephanalysis is drawn separating overcast, broken, and clear to scattered areas. Fog and sky-obscured reports are considered as overcast. The lack of data over oceanic and tropical areas is a limiting factor to both composite analyses.

First the radiation maps were drawn as completely and independently as possible. The composite nephanalyses were then drawn. In the areas north of 35° N. to 40° N., where there were sufficient data for independent radiation and nephanalyses, the close relationship between the two analyses was apparent. Hence the nephanalysis, where available, was used to supplement the radiation analysis in those areas where data were sparse. While not an ideal method, it was considered best in these few, early radiation maps to permit as much study as possible of their potential value. With increased density of radiation observations, a completely independent radiation map could be drawn.

It is interesting to note that in those large sections of the oceans and Tropics where there are no surface observations for a nephanalysis, the major source of data was the satellite radiation observations. Because of the large gaps between orbit paths in the Tropics, interpolation in drawing isolangleys is difficult. Here 24-hour continuity in radiation observations proves invaluable.

3. RADIATION MAP FEATURES AND RELATIONSHIPS

The fact that clouds dominate in determining the radiation pattern is apparent when comparing the radiation analyses (figs. 1, 4, and 7) with the nephanalyses (figs. 2, 5, 8) in those areas north of 40° N. where data were sufficient for their independent analysis. Since most mid-latitude extensive cloud systems of variable vertical development are caused by surface low pressure centers and fronts, the resulting radiation map patterns also reflect these sources. Where the surface Low or front is most intense, the cloud tops are higher and colder, and the outgoing long-wave radiation is less. As the cloud tops lower, the radiating temperature rises and the amount of radiation measured by the satellite sensor increases. On the radiation map this results in a radiation Low over the area of maximum cloud development, and higher isolangley values over the area of lower cloud tops. The highest radiation readings are found over

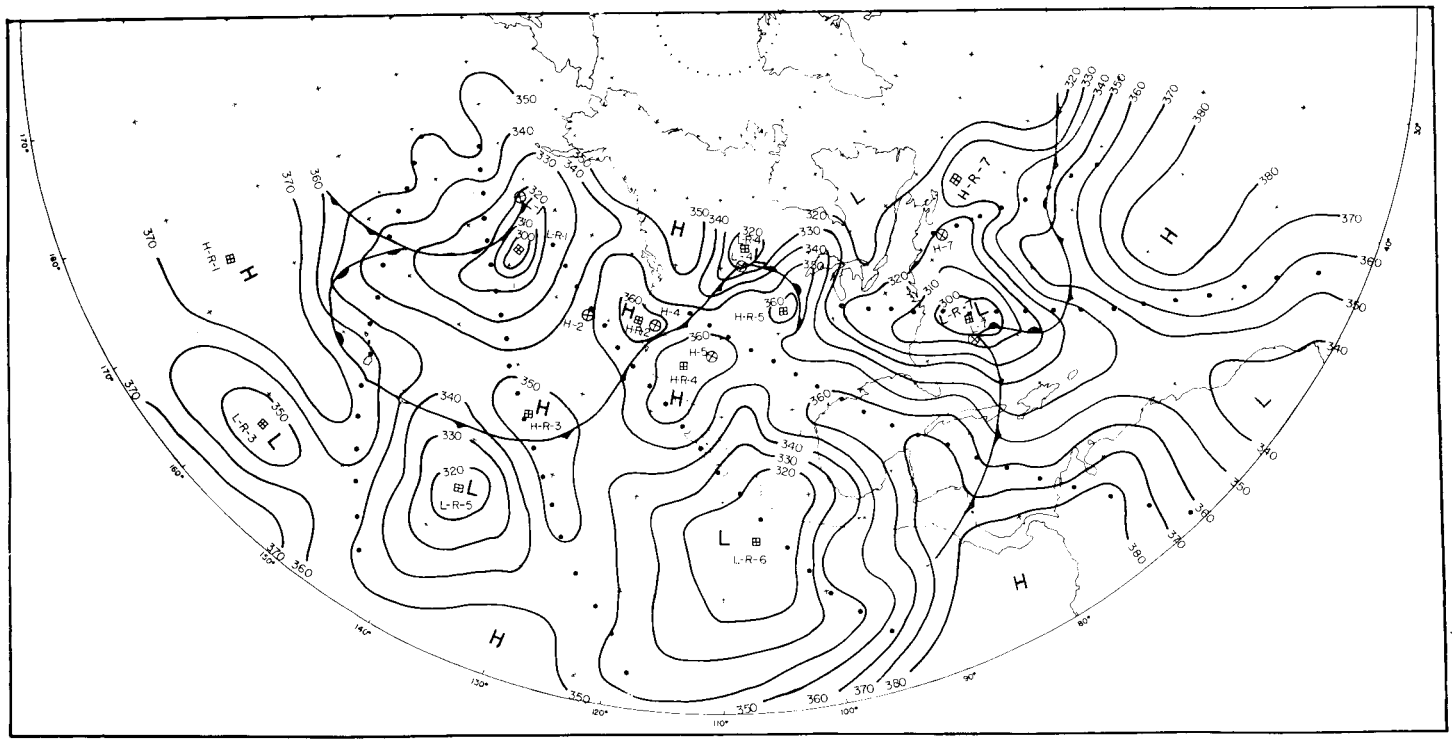

FIGURE 7.—Long-wave radiation loss map, December 3, 1959. (See fig. 1 for legend.)

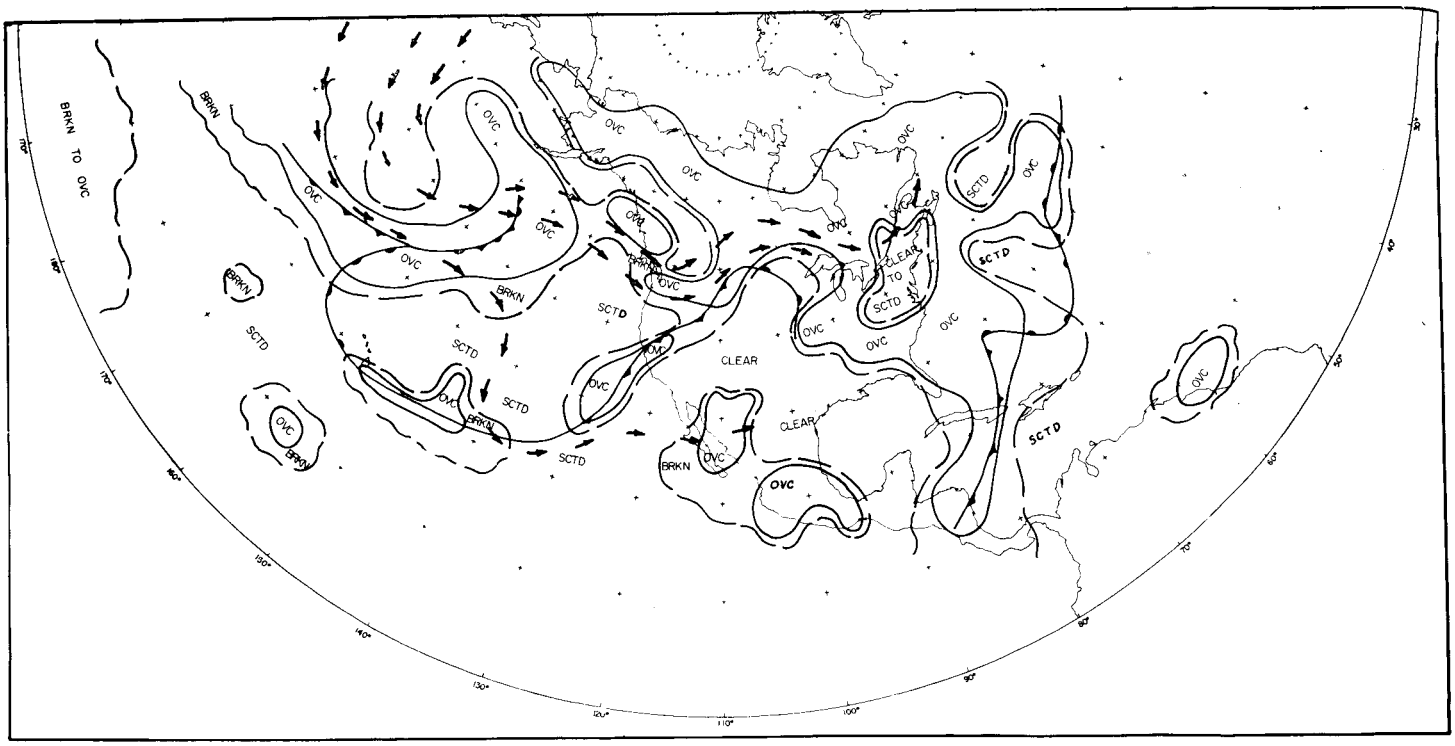

FIGURE 8.—Composite nephanalysis, December 3, 1959. (See fig. 2 for legend.)

the central and eastern sections of surface Highs where clear to scattered conditions generally prevail.

From the above relationships, one would expect to find the radiation low center east of the mid-latitude surface low center and the radiation high center east of the mid-latitude surface high center; and one does find this occurring in 24 of the 25 cases for which data are available (fig. 11).

An example of the usual relationship is radiation Low L–R–1, located southeast of surface Low L–1 and the associated Pacific occlusion on December 3, 1959 (fig. 7). It is interesting to note that the orientation of the radiation

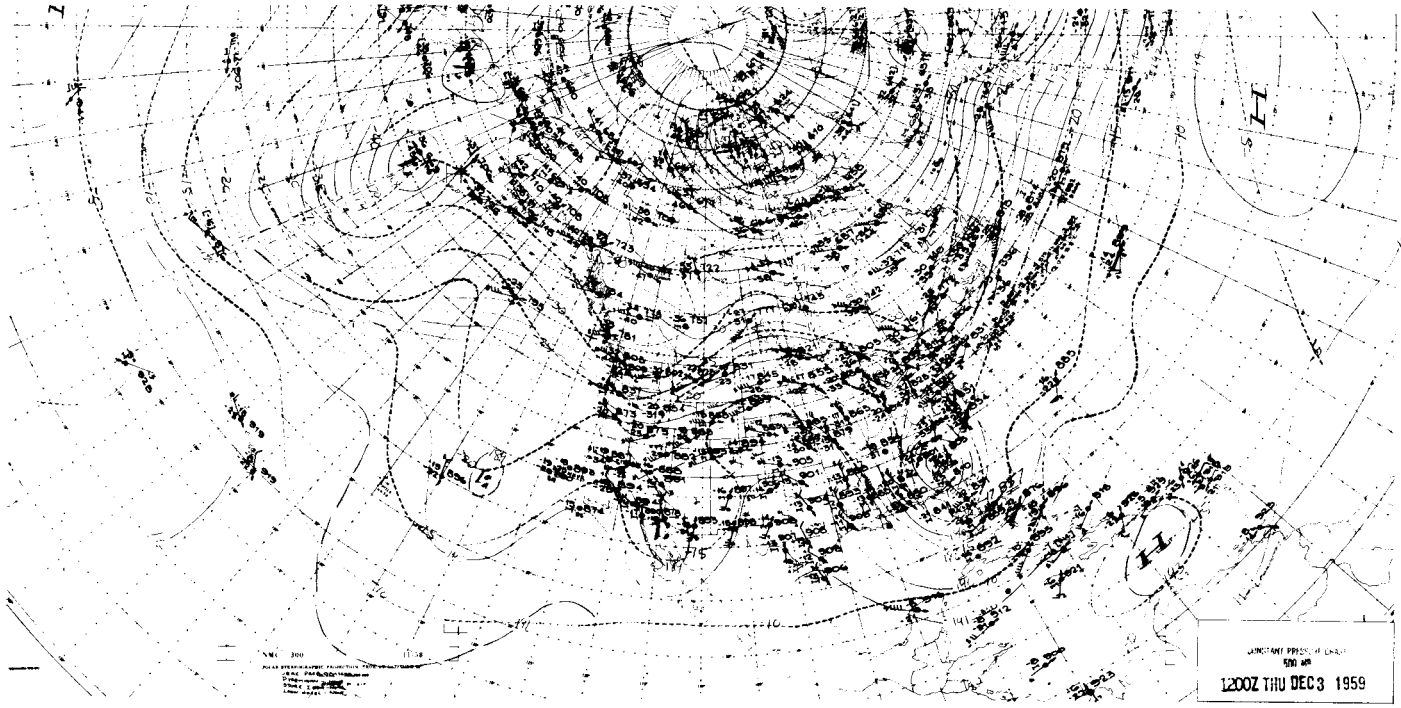

FIGURE 9.—500-mb. map, 1200 GMT, December 3, 1959.

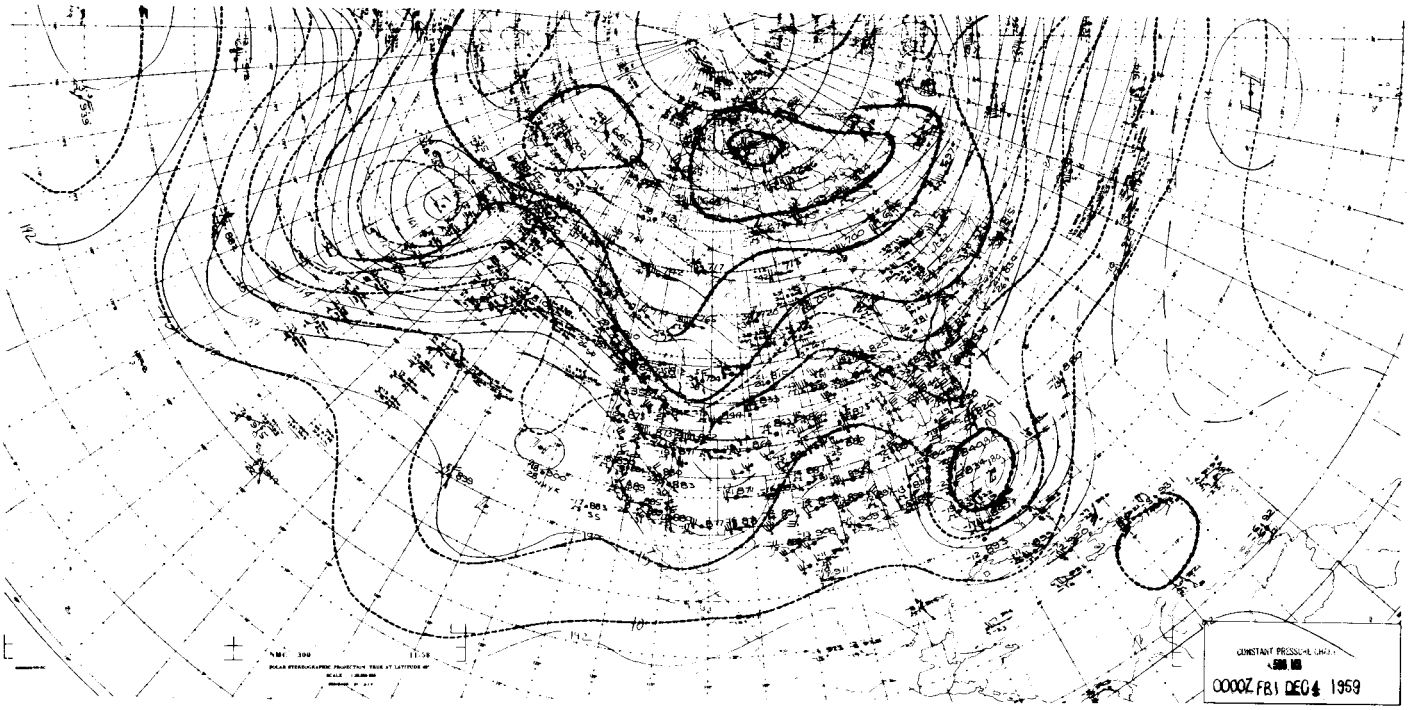

FIGURE 10.—500-mb. map, 0000 GMT, December 4, 1959.

Low and trough parallels the occlusion and area of maximum intensity, and the radiation pattern's spiral-like extension northwestward resembles TIROS cloud photographs of occlusions.

In addition to frontal location, the radiation trough, by its sharpness and strength of isolangley gradient, indicates frontal intensity, and by the interdiurnal change in these criteria, 24-hour frontal changes. An example is the cold front which starts in northwestern Canada from the remnants of an old occlusion and extends southwestward into the Pacific (fig. 1). The radiation map correctly indicates that the front is stronger in the region where its clouds produce L–R–4 and the sharp radiation trough to its southwest, weaker through the area

where radiation High H–R–3 reflects only clear to scattered clouds (fig. 2), and again more intense as it becomes a warm front leading into the unstable wave of surface Low L–1 where the radiation trough strengthens toward L–R–1. The weakening of the radiation trough off the Pacific coast on December 2 (fig. 4) reflects the decreased activity of the surface cold front.

The entire radiation trough pattern from L–R–4 to L–R–1 and then southwestward resembles a cyclone "family" and, in fact, is the radiation map reflection of one. The development of family "member" L–1, from an unstable wave to an occlusion can also be followed on the radiation maps during the succeeding days.

The arrows representing the pattern and location of maximum winds on the U.S. Weather Bureau 0000 GMT 300-mb. maps have been plotted on the nephanalyses. On December 1, 1959, (fig. 2) the maximum upper wind and frontal patterns conformed to that given by [10] and [2] for the relationship of the jet stream to a cyclone family. Again, the radiation patterns of Lows and troughs show the same relationship to the jet stream as do the surface Lows and fronts of the cyclone family.

While a radiation Low is usually the reflection of a surface Low or front, it can also be caused by a cold or snow surface or an extended sheet of high clouds. Both of these sources may generally be distinguishable by radiation map analysis and continuity. There are no snow surfaces indicated in this series of maps. However, it is very likely that extended sheets of high clouds caused the tropical radiation Lows which are not related to identifiable synoptic features. Such large areas of high clouds in the Tropics have been reported by [1, 7, 5, 9]. It is felt that if there were sufficient radiation observations above an easterly wave, the resulting radiation pattern would show a minimum over the high clouds in the convergence area. Synoptic data available do not indicate any easterly waves for these dates.

4. 24-HOUR CHANGES IN INTENSITY

During the intensification of a surface or upper air Low there is an increase in size, vertical development, and meridional expansion of the cloud pattern. These changes are reflected in the radiation pattern.

The changes in value of the radiation center reflect the interdiurnal change in intensity of its surface counterpart for five of eight high centers and four of six low centers studied here (figs. 11a and b). Reasons for the "misses" are difficult to determine but some possiblities are: the pressure changes may have been too small to result in changes in clouds and radiation intensity; the clouds may already have been at maximum height. From the limited examples available, one can say that in all four cases when the 24-hour change in magnitude of the surface Low was greater than 10 mb., the change in radiation Low intensity was in the same sense.

Intensification of a surface center is also indicated by 24-hour shifts in the relative positions of its related radiation center. For example, radiation Low L–R–7 moved from southeast to north-northeast of its intensifying surface Low from December 2 to 3, 1959 (fig. 11a). Limited data in the Pacific indicate that L–R–1 was located east-southeast of surface Low L–1 on December 1, moved to its east-northeast on the 2d, and then to its southeast after occlusion took place. On both dates L–1 deepened. Reasons for the last change are not readily apparent. With an intensifying system such as L–1 moving northeastward, one would normally expect some northward motion of the radiation Low relative to the surface Low, reflecting the movement of highest clouds. However, in this case, the radiation Low and trough were apparently in the region of most intense convergence and vertical motion just ahead of the surface position of the occlusion (figs. 7, 9, 10). It was also noted in the few available cases that radiation Lows related to surface Lows which were weakening or not changing retained their same relative position. L–2 and L–4 and their radiation Lows are good examples.

TABLE 1.—*Surface and radiation center motions*

Radiation center	24-hr. motion (kt.)	Surface center	24-hr. motion (kt.)	500-mb. geostrophic wind	
				At radiation center location (kt.)	Padiation center motion/V_g (percent)
December 1–2, 1959					
H–R–1	E 11	None			
H–R–2	E 22	H–2	ENE 25	W 40	55
H–R–3	SE 19				
H–R–4	NE 20	H–4 to H–2	E 7	Light	
H–R–5	S 16	H–5	SSE 16	NNW 35	46
H–R–6					
H–R–7	ESE 21	H–7	ESE 22	NW 45	45
L–R–1	NE 26	L–1	ENE 24	WSW 45	53
L–R–2	E 35	L–2	E 35	WSW 60	58
L–R–3	E 15				
L–R–4	ENE 26	L–4	ENE 36	SW 65	40
L–R–5	NNE 19				
L–R–6	E 25				
L–R–7	ESE 15	L–7	SE 14	W 35	43
L–R–8					
December 2–3, 1959					
H–R–1	E 11				
H–R–2	E 29	H–2	ENE 32	WNW 50	58
H–R–3	SE 27				
H–R–4	NE 20	H–4 to H–2	NE 22	NW 20	100
H–R–5	SE 10	H–5	SE 11	NW 30	33
H–R–6					
H–R–7					
L–R–1	NE 36	L–1	NE 42	SW 80	45
L–R–2					
L–R–3	E 17				
L–R–4	ENE 31	L–4	E 35	WSW 75	41
L–R–5	NE 18				
L–R–6	E 15				
L–R–7	SE 39	L–7	SE 42	Upper Low extends to 300 mb.	
L–R–8	ESE 11	L–8 to L–7			

Another indication of surface Low intensification, based on radiation map data *alone*, is the change in orientation of a radiation low pattern from east-west to north-south coupled with a decrease in magnitude of the radiation center. This occurred with L–R–1 and L–R–7 over the 3 days of maps. The reverse applies to a weakening system, as exemplified by L–R–2 and L–R–4.

5. 24-HOUR MOTION AND 500-MB. GEOSTROPHIC FLOW

Figures 11a and b and table 1 show a possibly useful

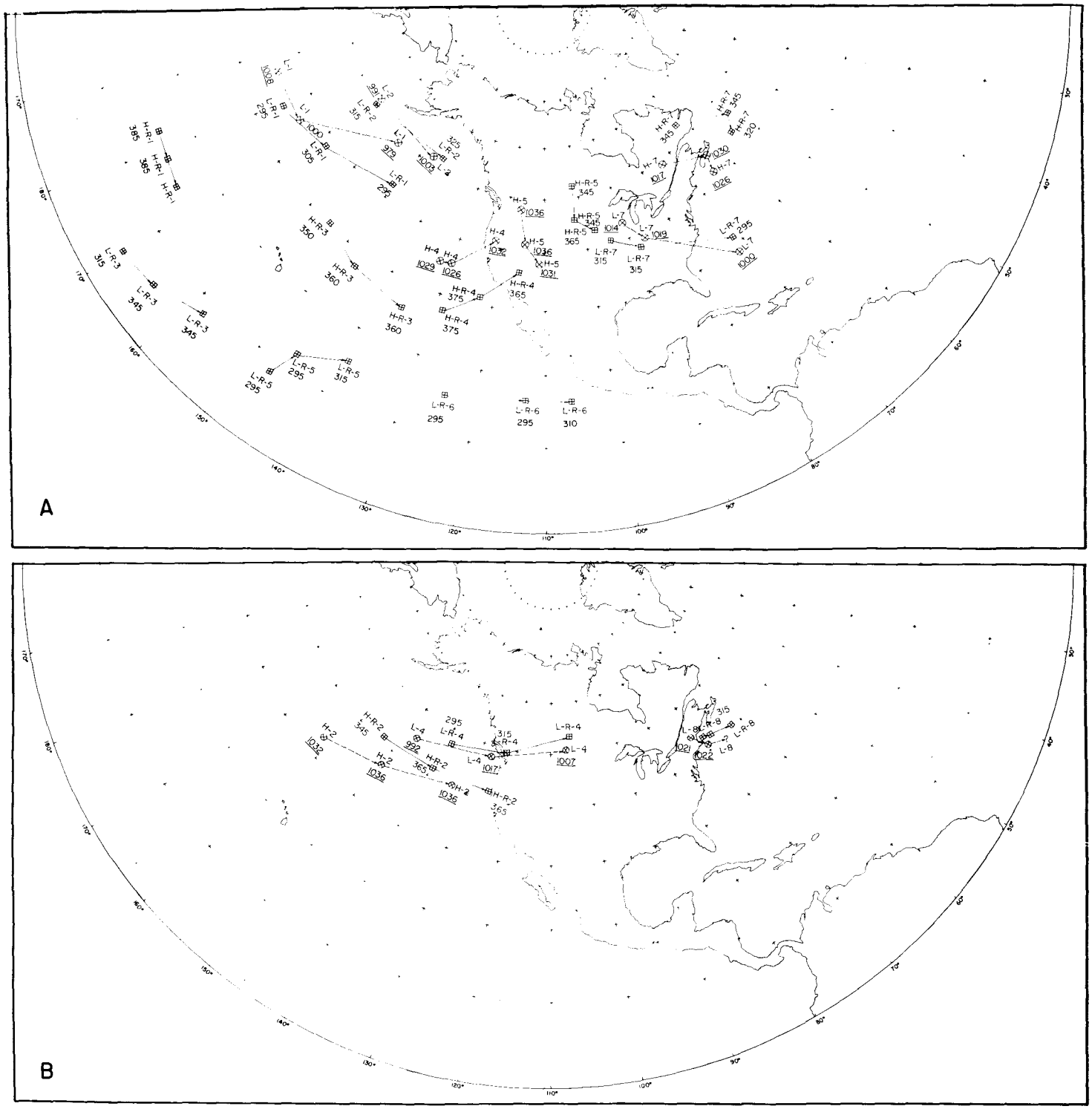

FIGURE 11.—(a) Surface and radiation center continuity, December 1–3, 1959. The surface pressure center locations are indicated by circles, their values in millibars are underlined, and their 24-hour locations are connected by a dashed line. The radiation center locations are indicated by squares, their values are in Langleys per minute $\times 10^{-3}$, and their 24-hour locations are connected by a solid line. (b) Additional surface and radiation center continuity, December 1–3, 1959.

relationship between the interdiurnal movements of the mid-latitude surface and associated radiation Lows and Highs. The 24-hour motion of six of the seven radiation Highs available for study was within about 20° and 10 kt. of that of their related surface system. The seventh example, comparing the motions of H–R–4 and H–4, is complicated by H–4's becoming absorbed in surface High H–2. The 24-hour movements of *all seven* radiation Lows followed that of their surface Low within these same limits.

A positive relationship is found between the 24-hour motion of the radiation low center and the average 500-mb. geostrophic wind velocity over its area of motion.

613342—61——2

Computations were made from contour spacings on the National Weather Analysis Center 500-mb. maps for December 1 through 4, 1959 (figs. 3, 6, 9, 10). The motions of four of seven radiation Highs were within 20° of the direction and between 40 and 60 percent of the speed of the related 500-mb. geostrophic wind velocity (table 1).

The radiation Lows' motions show even better correlation. *Six of the seven cases* for which data are available were within these limits. The seventh case involves the intense surface Low L–7 and radiation Low L–R–7 on December 3. A closed Low also developed in the upper air maps to at least 300 mb. (highest level available for study) and hence the 500-mb. level cannot be considered a "steering" map for that system.

These results indicate that the radiation low center's motion could be used to determine the 500-mb. flow pattern, and the approximate location of the corresponding surface Low center, its movement, and possible changes in its intensity.

The cirrus clouds causing the tropical radiation Lows were probably between 12 and 16 km. Although the 500- and 300-mb. analyses extend only to 15°–20° N., the contour pattern indicates the westerly flow continued farther south at these and higher levels, causing the generally eastward motion of H–R–1, L–R–5, and L–R–6. L–R–3 could have been under the influence of the equatorial westerlies which, according to [6], can extend. to 16 km. These subtropical centers also showed good continuity (fig. 11a).

6. CONCLUSIONS

The relatively simple omnidirectional white radiation sensor aboard Explorer VII measures long-wave radiation at night which, when converted to Langleys per minute, can be used to produce radiation maps. In mid-latitudes, where adequate data exist, the radiation pattern is consistent with the nephanalysis pattern and with synoptic features. Analysis techniques are similar to those presently used for surface and upper air maps.

The radiation map appears to offer many aids to analysis and forecasting, particularly for areas of sparse data, which should be confirmed by further study. Best results are for the mid-latitude low center relationships. The radiation low center gives an approximation of the location, motion, and change of intensity of the surface low center. In addition, in limited areas where the direction of motion of the radiation Low is available, the upper air pattern and 500-mb. winds may be approximated. A special synoptic situation, the cyclone family, is recognizable and the general location of the associated maximum winds may be determined. In all latitudes the radiation analysis whether determined by radiation data alone, nephanalysis alone, or a combination of both, shows good continuity (figs. 11a and b).

It may also be possible to determine vertical motion patterns from the radiation map patterns, particularly when combining the low resolution, quantitative radiation map figures from Explorer VII with the high resolution, qualitative cloud pictures from TIROS. Research on this relationship is being conducted at the University of Wisconsin.

Radiation measurements from two satellites in polar orbits would increase observation density and make the maps more nearly synoptic, increasing their accuracy and value. Data storage capability aboard a single satellite would make it possible to have radiation maps for the entire earth using just single, or a few, readout stations.

The conclusions arrived at are based on data not always as complete as desirable and on maps which are both nonsynoptic and few in number. However, these limitations are mitigated by the consistency of the relationships over the 3-day period and, in the northern latitudes, by the density of radiation observations which lessened subjectivity.

ACKNOWLEDGMENTS

It is not possible to acknowledge individually the very many persons who made the satellite flight, data collection and reduction, and radiation map analysis possible even though their contribution is enormous. To avoid any possible unintentional omission we wish to acknowledge the large contribution and support given by the National Aeronautics and Space Administration, the National Academy of Sciences, the U.S. Weather Bureau, the University of Wisconsin, and the U.S. Air Force Air Weather Service.

REFERENCES

1. A. E. Cole, "Clouds," *Handbook of Geophysics for Air Force Designers*, 1st Ed., U.S. Air Force, Geophysics Research Directorate, 1957, pp. 7–1—7–7.
2. A. H. Glaser, "Meteorological Utilization of Images of the Earth's Surface Transmitted from a Satellite Vehicle," Report under contract AF 19(604)–1589, (AFCRC TR–57–241, ASTIA–AD–146764), Harvard University, Blue Hill Meteorological Observatory, Milton, Mass., 1957, 145 pp.
3. L. Holloway, "Correcting for Unavoidable Smoothing of Artificial Satellite Data," Paper presented at 155th Meeting, American Meteorological Society, Washington, D.C., April 29–May 2, 1957.
4. F. B. House, "On the Interpretation of Long-Wave Radiation Data from Explorer VII Satellite," Paper being prepared at University of Wisconsin, Department of Meteorology, Madison, Wis.
5. H. M. Johnson, "Use of Satellite Data in Tropical Meteorology," Semiannual technical summary report No. 1, contract AF 19(604)–6156, prepared for U.S. Air Force, Geophysics Research Directorate, Bedford, Mass., July 1960, 25 pp.
6. C. E. Palmer, "The General Circulation between 200 mb. and 10 mb. over the Equatorial Pacific," *Weather*, vol. 9, No. 11, Nov. 1954, pp. 341–349.
7. R. G. Stone, "A Compendium on Cirrus and Cirrus Forecasting," *Air Weather Service Technical Report 105–130*, U.S. Air Force, Mar. 1957, 156 pp.
8. V. E. Suomi, "The Thermal Radiation Balance Experiment on Board Explorer VII," Chap. 11 in *JUNO II Summary Project Report*, vol. III, Explorer VII, NASA, George C. Marshall Space Flight Center, Huntsville, Ala., 1960, pp. 247–278.
9. V. E. Suomi and P. M. Kuhn, as yet untitled paper on infrared radiometer soundings in the Caribbean, 1961.
10. J. Vederman, "The Life Cycles of Jet Streams and Extratropical Cyclones," *Bulletin of the American Meteorological Society*, vol. 35, No. 6, June 1954, pp. 239–244.